Check for updates

Tailoring the optical properties of polyvinyl alcohol-polyvinyl pyrrolidone based polymers

Michael Gad[1] · Mohamed Elkattan[2]

Abstract

In this work, new polymeric based films are fabricated and optically characterized. The new films include poly(vinyl alcohol), plain and blended with poly(vinyl pyrrolidone), comprising glycerin, and acetic acid,as additives. XRD and FTIR analysis were conducted to give insight into the structure of the films. The reflectance and transmittance for these films are measured in the UV–vis–NIR regions. Using these measurements, the refractive index, the permittivity and many other optical constants are retrieved. The results reveal that the fabricated films possess an extinction coefficient that is almost 3 times less, and a refractive index that is 0.1 higher than plain PVA in the telecommunications wavelength range. Besides, a noticeable increase in the refractive index of the films is achieved, up to 0.35 higher compared with silicon dioxide at the near infrared spectral region. Moreover, when compared to silicon and Germanium, in the ultraviolet and visible spectral region, a substantial reduction of 3 to 4 orders of magnitudes in extinction coefficient is achieved, in the favor of the investigated films. Interestingly, the films also show small dispersion over a wide range of wavelength. Therefore, the newly proposed films can be candidates for opto-electronics, solar cells, and integrated optics applications where high refractive index and low loss are desired for high density of fabrication.

Keywords Dispersion · Nonlinear optical · Optical constants · Refractive index · Permittivity · Polymers

1 Introduction

Recently, polymers have drawn a lot of attention in the development of many opto-electronic and microelectronic devices (Liang and Wang 2016; Shen et al. 2017; Jiang et al. 2020). Polymeric materials have been introduced in integrated capacitors (Tan 2020), light detectors (Yang and Ma 2019), memristors (Yalagala et al. 2019), light-emitting diodes (Lee et al. 2019), optical circuits (Nocentini et al. 2018), laser

✉ Michael Gad
   mmonirmo@eng.asu.edu.eg

1   Engineering Physics and Mathematics Department, Faculty of Engineering, Ain Shams University, Cairo, Egypt

2   Department of Electronics, Nuclear Materials Authority, Cairo, Egypt

technology (Wei et al. 2019), optical waveguides (Oh et al. 2016), and electro-optic modulators (Gad 2007; Gad et al. 2008), among other devices. One of the distinctive advantages of polymers is that they can be doped with different additives to produce new composites with tailored physical properties (Abdel-Aziz et al. 2021; Deshmukh et al. 2017; Dhayal et al. 2021; Jilani et al. 2021). Consequently, characterization of the optical constants of the polymeric composites is critically needed in order to evaluate the modification and improvement in their electronic and optical properties.

Poly(vinyl alcohol) (PVA), as one of the most widely used polymers (Abdelrazek et al. 2010), has recently received considerable interest, owing to its numerous potential applications in optical components. PVA exhibits a semi-crystalline structure and is comprised of carbon chain backbone with hydroxyl groups attached to methane carbons (Al-ramadhan et al. 2016). One of the motivations to use PVA in this work is that its physical characteristics are impacted by the presence of OH groups, where the two-dimensional hydrogen bonding of PVA facilitates the development of polymer composites when it reacts with other functional polymers.

On the other hand, polyvinylpyrrolidone (PVP) is one of the attractive synthetic polymers that has carbonyl groups and pyrrolidone rings within its structure (Sreekanth et al. 2019). PVP is characterized by its amorphous nature and has a peptide bond in its lactam ring, making its side groups flat and extremely polar. PVP has been used in this work due to its favorable properties that includes an active charge transport mechanism, and good film- forming capabilities. The presence of the rigid pyrrolidone group in amorphous PVP helps provide better ionic mobility in the systems, while the carbonyl group (C=O) attached to the side chains of PVP helps in the formation of many complexes with different polymers.

One of the significant techniques for developing polymeric composites is polymer blending. Polymer blending is combining two or more polymer types in order to prepare a novel composite with features different from those of its individual constituents. Blending of PVA with PVP results in interaction between the -OH group of PVA and the C=O group of PVP via hydrogen bonding (Hashim 2020). This contributes in the formation of a stable blend with good film morphology and high flexibility in hosting different additives. Incorporations of various additives to PVA/PVP polymeric blend have been reported recently to demonstrate the change in various optical characteristics of the resultant composites (Badawi 2020a; El-naggar et al. 2022a, b, c).

In this paper, different films based on PVA/PVP polymeric blend are fabricated, structurally identified, and then their optical properties and constants are studied to demonstrate the induced changes in various optical characteristics of the resultant composites. The attained results reveal that all the studied optical parameters are affected by the different introduced additives, as compared with those of the plain PVA. Such change of properties enables polymers to serve in different applications such as integrated optics (Gad 2007; Gad et al. 2008), and solar cells (Heiba et al. 2021b).

The rest of the paper is organized as follows. Preparation of the polymeric composite films is detailed in section two. After that, a thin-film multiple-reflection model is employed in section three to deduce the main optical properties, i.e., the refractive index and permittivity from the transmittance and reflectance measurements. The optical parameters which describe the refractive index dispersion are discussed in section four, while the electronic losses and nonlinear optical properties are studied in section five. Finally, the conclusions are presented in the sixth section.

2 Polymeric films preparation and characterization

In this paper, four polymeric composite films are fabricated, and their optical constants are investigated. The first one, S1, is a plain poly(vinyl alcohol) (PVA) film. The second film, S2, is composed of 1% acetic acid embedded in poly(vinyl alcohol)- poly(vinyl pyrrolidone) polymeric host. The third film, S3, is composed of 1% glycerin embedded in poly(vinyl alcohol)- poly(vinyl pyrrolidone) polymeric host. The fourth film, S4, is composed of both 1% glycerin, and 1% acetic acid, embedded in poly(vinyl alcohol)- poly(vinyl pyrrolidone) polymeric host. The changes of the optical properties of the prepared composites are studied in the wavelength range $190\,nm \leq \lambda \leq 2500\,nm$ that is known as the ultraviolet–visible-near infrared (UV–vis-NIR) range.

The polymeric composite samples were fabricated via the solution casting technique based on the appropriate conditions for the composition synthesis that are altered to be chemically crosslinked. First, in order to obtain the first sample (S1), the PVA powder was dissolved in distilled water and stirred continuously for two hours at 70 °C until a clear transparent solution is achieved. Separately, the same procedure is done to obtain clear transparent PVP solution. PVA and PVP solutions were mixed together and stirred with a magnetic stirrer at 50 °C for two hours until a homogenous blend solution is achieved. After that, 1% acetic acid was added to the PVA-PVP solution blend, with continuous stirring at 50 °C, to obtain the second sample (S2). While separately, 1% of glycerin was added to the solution blend using the same procedure to obtain the third sample (S3). After that, and gradually, both 1% glycerin, and 1% acetic acid were added separately using a fine dropper to the PVA-PVP solution blend with continuous stirring at 50 °C, to obtain the fourth sample (S4). Finally, all the prepared solutions were cast into glassy petri dishes and left to be solidified in an oven for convenient time at 40 °C. The thickness for the formed samples is measured using a digital micrometer and is found to be 350 $\mu m \pm 1\mu m$. The thickness of the investigated films is adopted according to the compromise between the appropriate conditions for the composition synthesis to be chemically crosslinked, and the ease of applicability of the solution casting technique as a fabrication process.

X-ray diffraction (XRD) patterns of the fabricated samples were recorded at room temperature on a PANlytical Xpert PRO diffractometer of CuK$_\alpha$ radiation. ($\lambda = 1.54060$ Å). XRD data were collected from $2\theta = 4°$ to $2\theta = 90°$ with a step size of $0.02°$, and a scan time step of $0.6s$. The instrument was operated at a $45kV$ voltage and $40mA$ current. The diffraction patterns are shown in Fig. 1.


Fig. 1 XRD pattern for the fabricated films
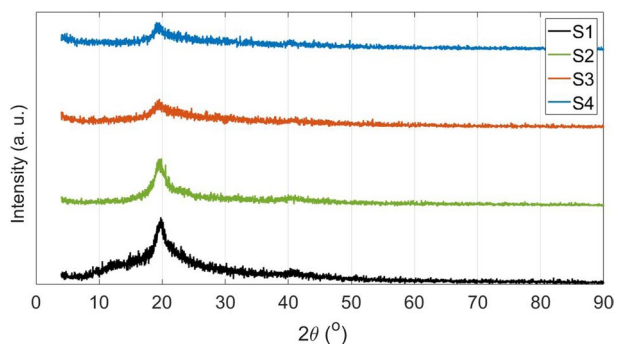
The pattern of plain PVA (S1) shows a well-defined relatively broad hump centered at $2\theta = 20°$ that characterize the semi-crystalline nature of the PVA (Ali and Kershi 2020; Ali et al. 2022)**.** It is observed that the intensity of the characteristic hump of PVA is decreased with adding acetic acid to PVP/PVP blend (S2). This confirms the interaction between the acetic acid and the blend, which results in destruction of the chains and decreases the semi-crystallinity domains of the blend (Abdolrahimi et al. 2018; Cholant et al. 2020). Moreover, a slight shift in the position of the hump peak is observed for S2 film to be around $2\theta = 19.16°$. This shift confirms the good compatibility and miscibility of the two polymer blend components due to the strong interactions between the polar function groups $-$OH of PVA and the C=O groups of PVP within the blend (Ali 2019).

Interestingly, the strength of the characteristic hump of PVA almost diminished with the loading of glycerin either alone (S3) or with acetic acid (S4) which indicates an increase in the amorphous nature of the polymeric composite (Choudhary 2018a). This confirms the dominant role of glycerin as a crosslinking agent in the blending process. The low molecular size of glycerin allows occupying intermolecular spaces between polymeric chains. This change the three-dimensional molecular organization of polymeric blend and reducing the energy required for molecular motion and the formation of hydrogen bonding between chains (Mohsin et al. 2011). Besides, the presence of hydroxyl groups in PVA creates a site for the crosslinking reaction, where, during the cross-linking process, the number of hydroxyl groups within the blend is depleted due to the complete cross-linking reaction, causing a strong complexation between the polymeric blend and the additive within the film, and consequently the increase of the amorphousness nature of the polymeric composite (Boonsuk et al. 2020; Cazón et al. 2019).

FTIR analysis is used to identify the functional structure of the fabricated polymeric films due to different additives and functional groups. Thus, it provides information about the crosslinking and interactions between various constituents and the complexations in the composites. Figure 2 shows the FTIR transmission spectra of the fabricated composite polymer films in the wavenumber range $4000 - 650$ cm^{-1}. The FTIR transmission spectra were measured using Agilent Cary 630 FTIR spectrometer.

The general insight of the FTIR spectrum of the fabricated polymeric films denotes observed variations in the positions and intensities of the characteristic bands as a consequence of the incorporation of the proposed additives into the PVA/PVP blend matrix. This clearly reveals the occurrence of polymer–additive interactions, and their impact of the functional structure of the fabricated polymeric films.

Fig. 2 FTIR spectra for the fabricated films
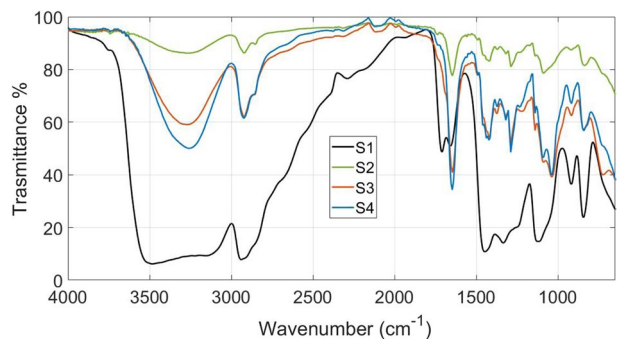
For the plain PVA film (S1), a wide broad band extended between $3000\,cm^{-1}$ and $3500\,cm^{-1}$ is observed, and it is correlated to the PVA main chain hydroxyl O–H stretching vibrational mode (Mansur et al. 2008). It is observed that this broad band becomes stronger and more defined, whereas, clear variations in the intensity of the band are noticed in the composite films, i.e., S2, S3 and S4 with respect to the plain PVA (S1). These results confirm that the proposed additives interact with the PVA chain, mainly with the hydroxyl group.

Another band centered at approximately $2928\,cm^{-1}$, which is usually observed in plain PVA spectra (Mohsin et al. 2011), denotes the C–H asymmetric stretching vibrational modes of PVA (Siva et al. 2021). This band becomes more intense with the presence of glycerin in S3, and S4 films which confirms the complexation of the different additives in the structure of the PVA backbone.

For S2, S3, and S4 samples, a band centered at approximately $2228\,cm^{-1}$, which observed usually in PVA/PVP blend spectra (El-naggar et al. 2022a, 2022b, 2022c), belong to C≡C bond. For plain PVA (S1) C=O stretching observed at the band in the range of (1664–1693 cm^{-1}). The position of this band is slightly shifted, for S2, S3, and S4 films, with variation of the intensity of the transmission value and its sharpness, when compared with S1 film. This reveals how different additives interact with the functional groups of the PVA structure.

For plain PVA (S1), multiple bands appeared between 1000 cm^{-1} and 1500 cm^{-1}, and are located at 1448 cm^{-1}, 1335 cm^{-1}, 1246 cm^{-1} and 1116 cm^{-1}. These peaks correspond to bending vibration mode of CH$_2$, (CH+OH) bending, CH wagging, and C–O stretching vibration, respectively (Badawi 2020b). On the other hand, For S2, S3, and S4 films, the observed bands at $1423\,cm^{-1}$ and $1289\,cm^{-1}$ correspond to the C=N (pyridine ring) and CH$_2$ twist vibrational modes, respectively, for pure PVP (Siva et al. 2021). Furthermore, the band at $1084\,cm^{-1}$ is likely associated with C–O stretching or O–H bending (Badawi 2020b). Moreover, in all investigated films, vibration bands at $924\,cm^{-1}$, and $842\,cm^{-1}$ are being ascribed to C–C, and –CH stretching vibrations, respectively, which is consistent with the vibrational modes of pure PVA (Choudhary 2018b).

Finally, From the FTIR analysis, the existence of these distinguishable vibrational modes of pure PVA and pure PVP films, with these shifts in the positions of the transmission peaks and the obvious differences in peak intensities and band sharpness; all emphasize the success of the interaction between the different additives in this work and the host PVA/PVP polymeric blend matrix. This interaction noticeably influences the backbone structure of the host polymeric blend which significantly affects the distribution of the potential energy along its chains (Dhahri et al. 2022; El Krimi and Masrour 2022).

Next, the results of the optical characterization of the fabricated thin films are shown. This includes measuring the transmittance, T, and reflectance, R, spectra. In these measurements, the diffuse reflection technique is adopted using V-570 (SLM-468) spectrometer from JASCO Corporation (https://jascoinc.com/). The measurements are realized in the UV–vis–NIR spectral range, where the wavelength, λ, ranges from 190 to 2500 nm, with a 2 nm resolution.

3 Refractive index and permittivity study

Analysis of the refractive index and extinction coefficient alongside permittivity values is a key factor to identify the optical characteristics of the fabricated films (Chapalo et al. 2020; Kleine et al. 2020). The complex refractive index, N, is defined as $N = n - ik$ where n and k give the real and the imaginary components. The real part

gives the phase variation of the optical wave propagating through the film, while the imaginary part, called the extinction coefficient, represents the propagation power loss. The spectral behavior of the refractive index can be estimated using the reflectance, R, and the transmittance, T, measurements of the fabricated films. To find the wavelength dependent N values, a thin-film multiple-reflection model is applied using the measured R and T values. First, let us build the required set of equations to describe the model. At the beginning, consider the case of a semi-infinite film. In this case, air of refractive index $N_1 = 1$ is the medium of the incident wave, while the polymer has a complex refractive index N_2. The power absorption coefficient, α, is defined as

$$\alpha = \frac{4\pi k}{\lambda} \tag{1}$$

Let the electric field of the incident wave from air onto the film be E_i, while the reflected field be E_r. Therefore, the field reflection coefficient for the semi-infinite film, r_{12}, is given by (Jacob et al. 2001):

$$r_{12} = \frac{E_r}{E_i} = \frac{N_o - N}{N_o + N} = \frac{1 - (n - ik)}{1 + n - ik} \tag{2}$$

The corresponding power reflection coefficient is R_{12}, where:

$$R_{12} = |r_{12}|^2 \tag{3}$$

From (2) and (3):

$$n = \frac{1 + R_{12}}{1 - R_{12}} \pm \sqrt{\frac{4R_{12}}{\left(1 - R_{12}\right)^2} - k^2} \tag{4}$$

The material we have is, on the other hand, in the form of a thin film not a semi-infinite one. And therefore, the effect of the multiple reflections should be taken into consideration. Hence, the measured reflectance, R, is related to the film thickness, d and R_{12} through (Jacob et al. 2001):

$$R = \frac{R_{12}\left(1 - e^{-2\alpha d}\left(2R_{12} - 1\right)\right)}{1 - R_{12}^2 e^{-2\alpha d}} \tag{5}$$

From Eq. 5, the power absorption coefficient, α, is found as follows:

$$\alpha = -\frac{1}{2d} \ln \frac{R - R_{12}}{(R - 2)R_{12}^2 + R_{12}} \tag{6}$$

The measured transmittance, T, for the thin film is given by (Jacob et al. 2001):

$$T = \frac{\left(1 - R_{12}\right)^2 e^{-\alpha d}}{1 - R_{12}^2 e^{-2\alpha d}} \tag{7}$$

Now that the model is established, the calculations required to retrieve the values of n and k from R and T will follow the next iterative procedure:

1. For each wavelength, λ, a value is assumed for R_{12} in the range $0 < R_{12} \leq R$. Let this value be R_{12}'.
2. Using the assumed R_{12}' value, along with the measured R and d values, a value for α can be calculated using Eq. 6. Call this value α'.
3. From Eq. 7, a value for T, call it T', can now be calculated using α', R_{12}' and d.
4. Then, let us define the percentage difference $a = |\frac{T-T'}{T}|$ and the allowed error limit, $b = 1\%$. If $a \leq b$ then the assumed value for R_{12}' and the corresponding calculated values α' and T' are acceptable and can then be used to calculate k from Eq. 1 and n from Eq. 4. If $a > b$, then these values are rejected, and the calculation process starts over with a new estimated value for R_{12}'. This iteration process keeps going until the condition $a < b$ is satisfied. Afterwards, the process is repeated for the next wavelength in the spectrum of the measurements.

The results of this calculation process are shown in the next figures. In Fig. 3, the measured transmittance, T, and calculated transmittance, T', are displayed for the four films. In Fig. 4, the measured reflectance, R, and the calculated R_{12} are shown for the four films. In Fig. 3, it is clear that the small difference $T - T'$ is a result of the condition set as $a = \left|\frac{T-T'}{T}\right| < b$ in the iterations. Since T is the measured transmittance and T' is the calculated transmittance from the model, then this algorithm proves very efficient in retrieving the transmittance values and hence assures the accuracy of the deduced values of other optical parameters as detailed next.

Also, the transmission spectra of the fabricated films show that the lowest transmission values along the whole investigated wavelength range is achieved when introducing 1% glycerin to the PVA-PVP host (S3). At the UV range (190–400 nm), all the fabricated films display the same behavior of increasing in T with the increase of the wavelength. At $400nm$, the transmittance dropped from 89% for the plain PVA (S1) to 32% for the PVA-PVP- 1% glycerin film (S3). Furthermore, compared with plain PVA (S1), samples S2 and S4 preserve the same high ($T > 80\%$), and wide transmission window in the range $400nm < \lambda < 1400nm$. At longer wavelengths ($\lambda > 1400nm$), T, for all the studied films, begins to diminish with the wavelength increase. At $1550nm$, T values are 75.98%, 79.67%, 56% and 75.79%, respectively, for S1, S2, S3 and S4 films.

The reflectance spectra in Fig. 4 reveal that introducing 1% acetic acid to PVA-PVP host (S2) results in a symmetrical $R(\lambda)$ variations, compared with the plain PVA (S1), except for higher reflectance values in the visible region (400−700 nm). On the other hand, adding 1% glycerin to the PVA-PVP host (S3), or combining 1% acetic acid with them (S4) results in an increase in R at both the UV, and visible regions, when compared with the plain PVA (S1). However, R values of both films (S3 and S4) begin to diminish gradually as the wavelength increases, until $\lambda > 2000nm$, where R values begin to rise again. At 1550nm, reflectance % values are 6.67%, 7.39%, 6.83% and 6.90%, respectively, for S1, S2, S3 and S4 films.

Next, we turn our attention to deducing the optical constants, based on the thin-film model. The calculated k values of the fabricated films are shown in Fig. 5. The results of k can be understood in light of the relationship between R_{12} and R shown in Fig. 4. Recall that R_{12} denotes the power reflection coefficient for the semi-infinite film placed in air. This means that when the difference between R and R_{12} is small, the thin-film multiple reflection effect is small. Therefore, the optical loss is high, meaning high k values and vice versa. And indeed, as shown in Fig. 5, the k-values are in general much lower in the range given
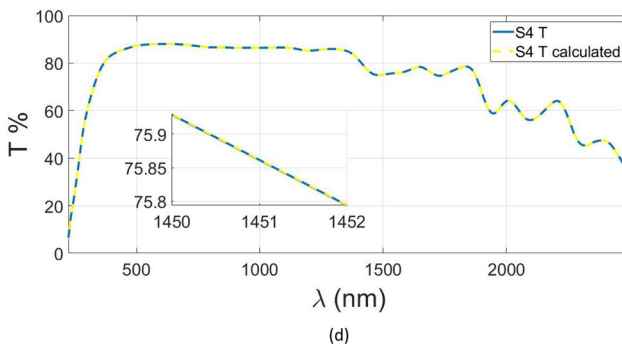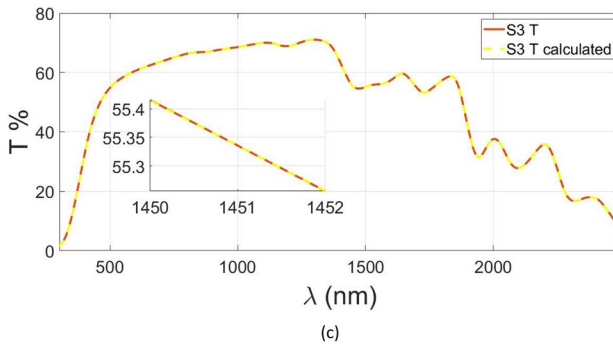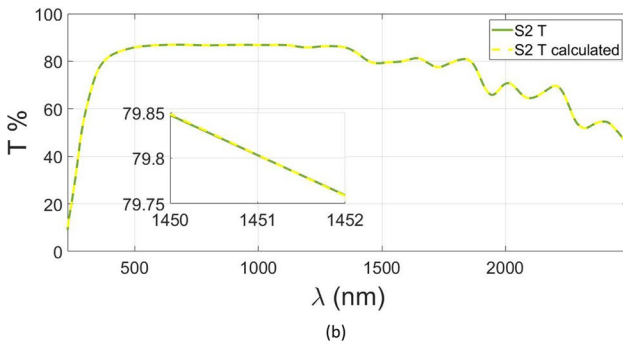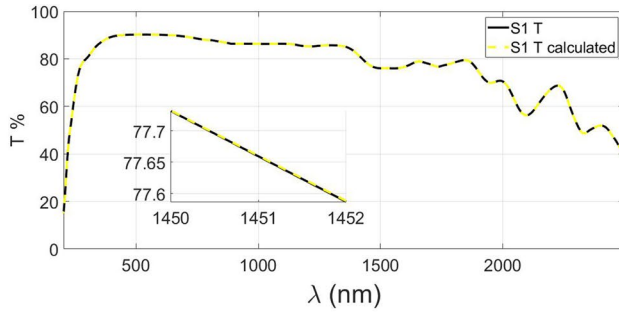
Fig. 3 The measured transmittance (T), and the computed transmittance (T') for (**a**) S1, (**b**) S2, (**c**) S3, and (**d**) S4 films. The inset shows how close the values of T and T' are

Fig. 4 The measured reflectance (R), and the computed semi-infinite film reflectance (R_{12}) for (**a**) S1, (**b**) S2, (**c**) S3, and (**d**) S4 films
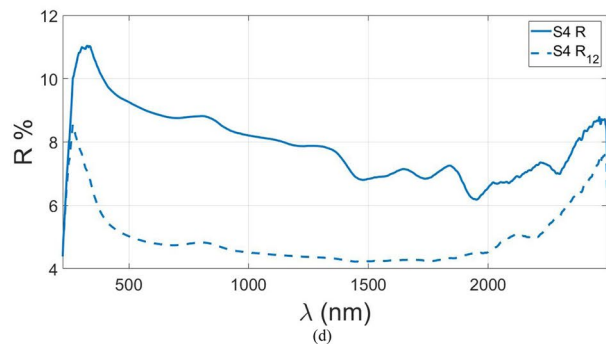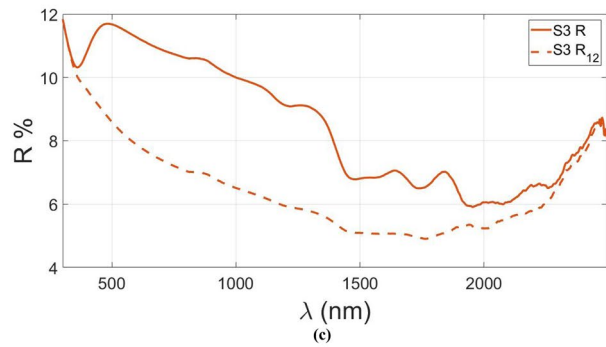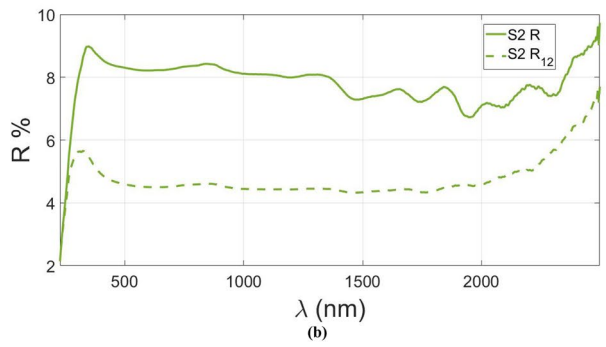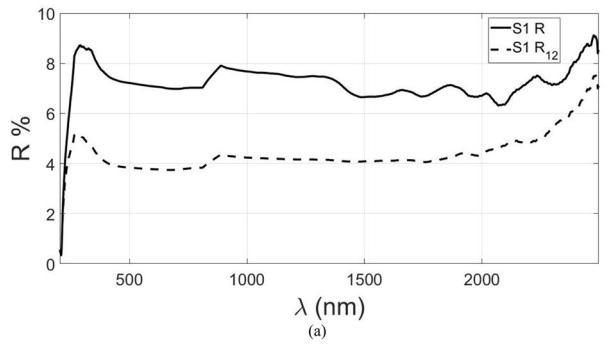
by 400nm $< \lambda <$ 2000nm than the rest of the spectrum. This is the range where $\frac{R_{12}}{R} <$ 70%. This also means that the samples are more transparent in the range 400nm $< \lambda <$ 2000nm, which is manifest in Fig. 3 with higher T-values in this range compared to the values outside this range.

Now, comparing the extinction coefficient values for the fabricated films we see in Fig. 5 that k values decrease by adding the acetic acid as in S2 or by adding glycerol as in S3. Including both acetic acid and glycerol into the PVA-PVP host, as in S4, results in moderate k values between that of S2 and S3. These variations in the behavior of k are due to the structural modifications of PAV-PVP host matrix associated with embedding different additives to the blend, which affects the quantity of energy absorbed when the electromagnetic radiation propagates through the film.

Interestingly, the extinction coefficient drops down to the range $\sim 5 \times 10^{-5}$ for S2 in the optical fiber telecommunications range (1450nm $< \lambda <$ 1620nm), as shown in the inset of Fig. 5. This is a three times reduction compared to the extinction coefficient of the PVA film, S1. This improvement can position this material as a potential candidate for optical telecommunications and integrated optics applications (Mohammed et al. 2022).

At $\lambda >$ 1700nm the differences in k vlaues between the fabricated films starts to grow, with the tendency to rise as the wavelength increases. The presented peaks in the NIR spectral range can be attributed to interband transitions between the Highest Occupied Molecular Orbital (HOMO) and the Lowest Unoccupied Molecular Orbital (LUMO) bands (Othayoth et al. 2020). Comparing k values of S2, S3, and S4 films, in Fig. 6, with plain PVP (König et al. 2014) reveals that the fabricated films in this work possess significant reduction in k at the visible region, with a reduction in k (for S2 film) ranging around 99.7%, in the visible region when compared with plain PVP.

On the other hand, comparing k values of S2, S3, and S4 films, with key materials in optoelectronic applications, such as silicon (Si) and Germanium (Ge) (Aspnes and Studna 1983), as shown in Fig. 7, shows a substantial reduction of 3 to 4 orders of magnitudes in k for all the investigated films, in the favor of the investigated samples. These remarkable reductions in the extinction coefficient values of the fabricated films are a noteworthy merit from the optical communications perspective in these spectral regions (Kim et al. 2005).
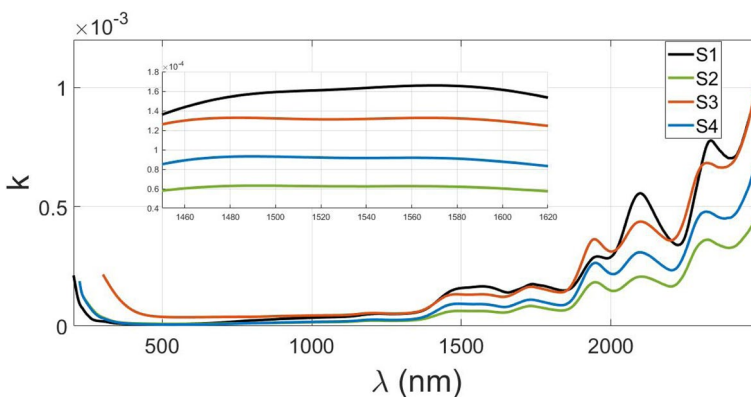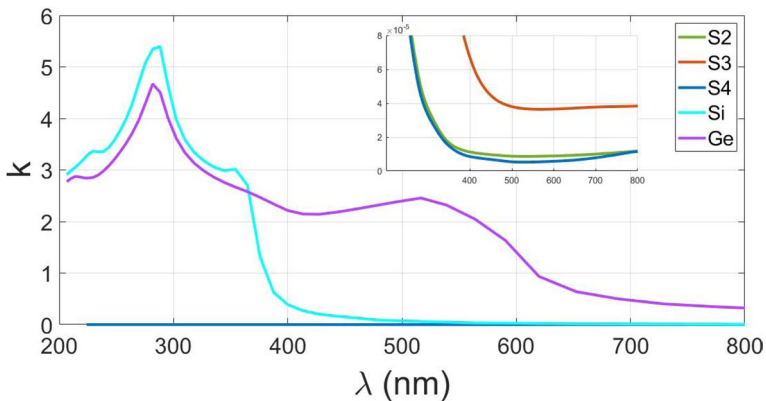

Fig. 5 The variation of extinction coefficient, k, with wavelength, λ, for S1, S2, S3 and S4 films. The inset reveals a zoom-in on the 1450$nm < \lambda <$ 1620nm range
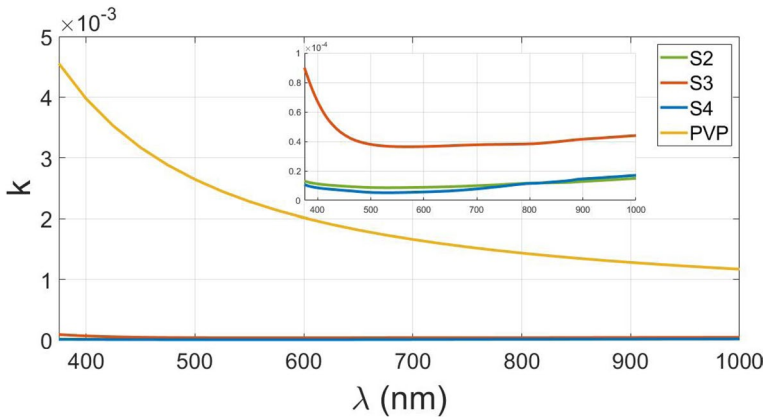
Fig. 6 A comparison of the extinction coefficient for the prepared films S2, S3 and S4 with PVP. The inset reveals a zoom-in on the results for S2, S3 and S4

Regarding the real refractive index, n, recently, high n polymeric composites have attracted a lot of consideration due to their role in the future optical system designs (Othayoth et al. 2020; Tang et al. 2020). The refractive index is an important optical parameter for describing the polarization behavior that occurs under the influence of the incident photons (Ali et al. 2022).
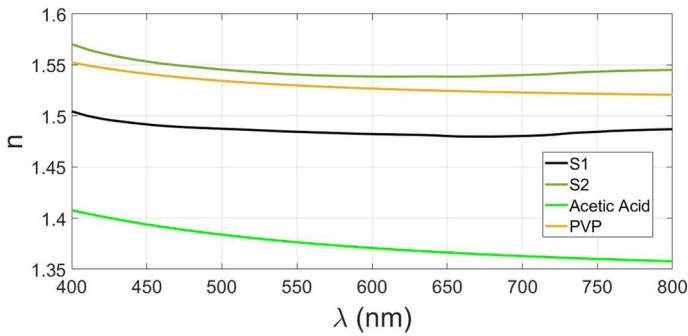
The real refractive index, n, values are deduced from the proposed thin film model results and are displayed in Fig. 8. The alternations in the n values of the different composites coincide with the existence of variations within the intermolecular polymer structure as proved in the FTIR results. Also, it is evident that the refractive index of PVA (S1) experiences a small increase by adding 1% acetic acid, as in sample S2 and also by adding 1% glycerol along with 1% acetic acid, as in sample S4. This may be ascribed to the interaction between the acetic acid and the polymeric blend, which results in suppressing the formation of new hydrogen bonding between polymeric chains. This leads to forming less compact structure, and hence, lower refractive index values. Yet, the refractive index of both

Fig. 7 A comparison of the extinction coefficient between the prepared films S2, S3 and S4 with Si, and Ge. The inset reveals a zoom-in on the results for S2, S3 and S4
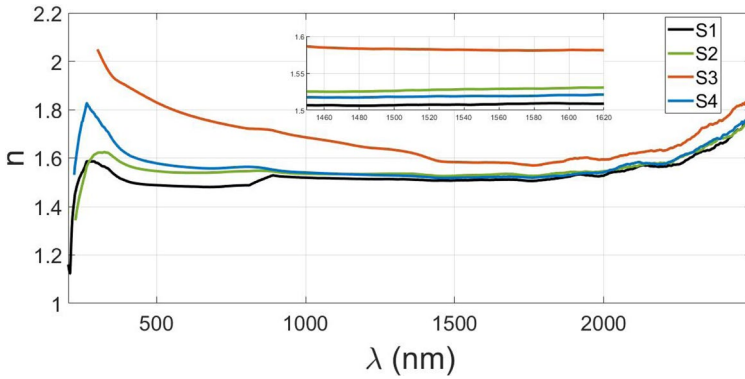
Fig. 8 The variation of the real part of the refractive index, n, with wavelength λ for S1, S2, S3 and S4 films. The inset reveals a zoom-in on the 1450nm < λ < 1620nm range

Fig. 9 A comparison of the real refractive index between S2 film and its individual constituents, PVA (S1), PVP (König et al. 2014), and Acetic acid (El-Kashef 2002)
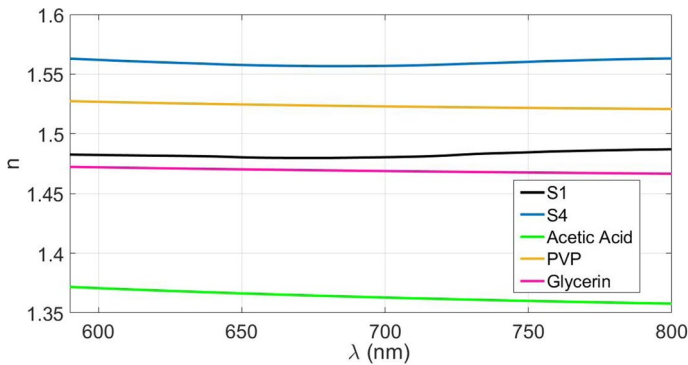
Fig. 10 A comparison of the real refractive index between S4 film and its individual constituents, PVA (S1), PVP (König et al. 2014), Glycerin (Rheims et al. 1997), and Acetic acid (El-Kashef 2002)

S2 and S4 films displays higher values than their individual constituents, especially in the visible region, as displayed in Figs. 9, and 10 respectively.

Back to Fig. 8, it is interesting to note that, adding 1% glycerol only to PVA-PVP host, as in sample S3, results in a strong rise in the refractive index, along the whole investigated wavelength range, between 0.05 and 0.4, when compared to plain PVA (S1). This is evidence for the formation of new intermolecular bonds between glycerol as a crosslinker and the PVA-PVP host matrix, which increases the density of chains packing of the blend and causes more impedance for the light within the designed blend film. This is coinciding with the transmission spectra of S3 film, which show the lowest transmission values, compared with the other films, along the whole investigated wavelength range.

Most importantly, in the optical telecommunications range, shown in the inset of Fig. 8, the increase in n is approximately 0.1. This is a good advantage in optical communications and integrated optics applications because a higher refractive index for the core of the waveguide, surrounded by a smaller refractive index cladding, enables a smaller radius of curvature (Gad et al. 2011b; Gad et al. 2008a, b). This means a higher density of device fabrication and hence a more compact optical circuit production (Pina-Hernandez et al. 2014). Another advantage shown in the same range is the almost flat $n - \lambda$ curves. This is an indicator of low dispersion which is also a highly desirable feature in optical circuits and telecommunications. With lower dispersion, the optical signal can travel a longer distance without the information being distorted. This means a lesser need for dispersion compensator components within the optical systems (Gad et al. 2009, 2011a).

Another important note in this study is the comparison between the real refractive index of S2, S3, and S4 films, and one of the most widely used materials in optical fiber and photonics applications, which is silicon dioxide (Labib et al. 2019a; b Mahrous et al. 2020a; Shalaby et al. 2019, 2020) (SiO_2). It was found that the fabricated films exhibit higher n values than those of silicon dioxide along the whole studied range in this work. The difference in n values between S2 film and silicon dioxide ranges between 0.14 at the UV, and visible regions, and 0.25 at the NIR region. For S3 film, the difference in n values become higher, and ranges between 0.4 at UV region, through 0.25 at the visible region, until it reaches 0.35 at the NIR region. At the fiber-optic telecommunications range, the difference between the fabricated films and silicon dioxide is about 0.1. This enables these polymeric composite films to be alternative candidates for applications that currently rely on silicon dioxide which is frequently used along with silicon in integrated photonics circuits (Gad et al. 2010; Mahrous et al. 2020b; Mahrous et al. 2020c; Mahrous et al. 2019; Shalaby et al. 2019).

Here, it is worthy to note that, generally, the reflectance and the transmittance for all films show their largest values in the UV region ($\lambda < 400$nm). Then, the reflectance tends to decay in the visible region (400nm $< \lambda < 700$nm) while the transmittance keeps high values. In the infrared region ($\lambda > 700nm$), the reflectance shows a tendency to grow, but not as in the UV region, while the transmittance shows a decay trend. This behavior follows from the optical properties of the films described by the refractive index and the permittivity, studied below. As explained by Lorentz model (Wooten 1972; Zappe 2010), high transmittance is associated with small extinction coefficient, k, values, which is the case in the UV and visible regions. Thus, the material changes to be reflective and then absorptive when k changes from small to large while n is large moving from the visible range deeper into the IR range.

The optical permittivity parameter is also another important property that must be investigated to suggest a suitable application. Study of the wavelength dependence of the permittivity is of high importance for the optical materials as it gives an insight about the
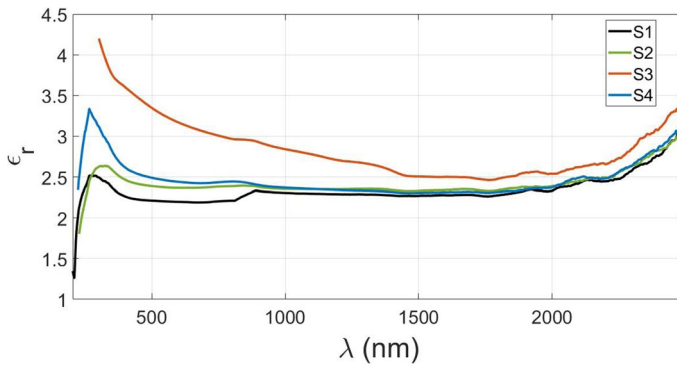
Fig. 11 Variation of the real part of the permittivity, ϵ_r, with wavelength for S1, S2, S3 and S4 films
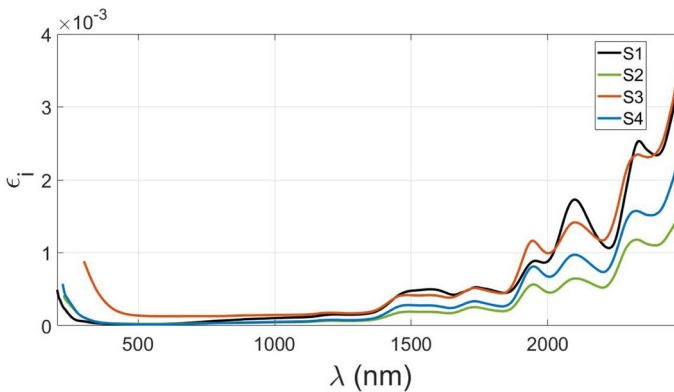
Fig. 12 Variation of the imaginary part of the permittivity, ϵ_i, with wavelength for S1, S2, S3 and S4 films

electron-photon interactions, and the consequent energy storage and loss inside the material (Akouibaa et al. 2022; Masrour et al. 2022; Sakli et al. 2021). The complex permittivity term ϵ serves as a key factor in the evaluation of other optical properties of the fabricated films, and is defined as: $\epsilon = \epsilon_r - i\epsilon_i$, where ϵ_r is the real part of the permittivity; $\epsilon_r = (n^2 - k^2)$, while ϵ_i is the imaginary part of the permittivity; $\epsilon_i = i2nk$ (Belhamra et al. 2022; Raïâ et al. 2022a).

Variations of ϵ_r and ϵ_i with wavelength for the fabricated films are displayed in Fig. 11, and Fig. 12, respectively. The alteration in the ϵ_r and ϵ_i values of the different composites can be attributed to the alteration in the number of oscillating dipoles, which causes a redistribution of electronic charges and, hence modification in the polarizability of the polymeric films (Aziz et al. 2021). Also, it is evident that the trends in ϵ_r spectra are similar to those in the real refractive index n spectra. This is mainly because the k^2 values are too small when compared with the n^2 values for all the investigated films. It can be seen in Fig. 11 that adding 1% acetic acid (S2), or both 1% acetic acid and 1% glycerin (S4) to the PVA-PVP host results in dispersive behavior at the visible region, while at higher wavelengths, ϵ_r values of both films are almost constant. At $\lambda > 2000$ nm, the ϵ_r values starts to increase again. On the other hand, adding 1% glycerin to the PVA-PVP host (S3) results in different ϵ_r behavior, where noticeably higher

values of ϵ_r are achieved, along the investigated wavelength range, compared with the plain PVA (S1). The increase of ϵ_r reveals the existence of more energy density of states within the polymeric composite and this results in an increase of polarization which gives the higher ϵ_r values (Aziz et al. 2017). This gives more favorable characteristics for S3 in applications that require energy storage (Mohanapriya et al. 2017; Morsi et al. 2022), and also supercapacitors applications (Kim and Lee 2020).

Here, it is noteworthy to mention that the permittivity behavior agrees with the expectations from Lorentz model (Wooten 1972). In the UV region, electronic polarizability plays a major role and is responsible for the high ϵ_i values in the range $\lambda < 400nm$. In the infrared zone, ionic vibrations are dominant and result in the oscillations of ϵ_i in the range $\lambda > 1500nm$. The visible range has no significant electronic, ionic or molecular resonances and therefore no big change shows on the values of permittivity ($\epsilon = \epsilon_r - i\epsilon_i$) or refractive index ($N = n - ik$) in this range.

When we look at ϵ_i spectra in Fig. 12, it is observed that at any wavelength, ϵ_r has much greater values as compared to ϵ_i for all the investigated films. The higher values of ϵ_r compared to these of ϵ_i confirmed the rise in the probability of occurring dispersion within the polymer matrix compared to the dissipation process of the incident electromagnetic radiation during the interaction process in the presence of different additives. This clearly indicates a remarkably less dissipation of energy inside the fabricated films (Chaabouni et al. 2022; Elkoua and Masrour 2022; Raïâ et al. 2022b). Furthermore, ϵ_i is relatively small in the range $400nm < \lambda < 1400nm$, which reveals a relatively low light loss. At $\lambda > 1400$ nm, the observed loss peaks at the end of the spectrum are reduced significantly, compared to plain PVA, S1, when 1% acetic acid is embedded inside the PVA-PVP host matrix, S2. The increase of ϵ_i at higher wavelengths ($\lambda > 1500$ nm) can be attributed to dipole polarization (Abdullah et al. 2015). As the wavelength decreases, the dipole polarization tends to be weak and thus ϵ_i values tend to be very small for all films.

4 Optical dispersion studies

Study of the dispersion behavior of optical materials is crucial due to its importance in optical communications performance and integrated optical devices design (Gad et al. 2017; Labib et al. 2019b). In order to correlate the previously attained optical constants in this paper to the dispersion parameters, first, the single-oscillator model by Wemple and DiDomenico is used to evaluate the energy dispersion of the optical parameters (Wemple et al. 1971). The proposed model descries the dispersion of the refractive index through the following formula (Naik et al. 2020):

$$n^2 = 1 + \frac{E_o E_d}{E_o^2 - E^2} \tag{8}$$

where E_o is the single oscillator energy which gives information about the average energy gap of the material, and E_d is the dispersion energy that gives information about the average strength of electronic transitions. The light photon energy, E, is given by $E = h\nu = \frac{hc}{\lambda}$ with $h = 6.63 \times 10^{-34} J.s$ being Planck constant, $c = 3 \times 10^8 \frac{m}{s}$ is the speed of light in space and ν is the photon frequency. To get E_d and E_o values, first, Eq. 8 can be re-formulated as:

$$\left(n^2 - 1\right)^{-1} = \frac{E_o}{E_d} - \frac{E^2}{E_o E_d} \tag{9}$$

Now, the values of E_d and E_o can be found by plotting $\left(n^2 - 1\right)^{-1}$ vs E^2, fitting a straight line to the high wavelength range points (towards $E = 0$), and then getting the line-intercept and the slope of the straight line. See Fig. 13. After that, the oscillator strength, $f = E_o E_d$ for the single oscillator model can be computed as well. The oscillator strength f describes the ability of the electrons of the initial and final states to absorb photon energy (Wemple et al. 1971).

E_d, E_o, and f values for the investigated films are listed in Table 1, where E_d and E_o identifies a strong connection to the variations associating with the structure of the material. It can be noted that E_o is the lowest for S3, when 1% glycerin is added to the PVA-PVP host. This reduction in E_o value can be attributed to decreasing of the energy and ionicity of the bonds inside the polymeric composite (Abd-Elnaiem et al. 2020) due to the increment in the degree of crosslinking when adding glycerin to the PVA-PVP blend. On the other hand, S4 film possesses the highest E_d value, suggesting an increase in the strength of inter-band optical transitions inside the film (Aziz et al. 2021) confirming the forming of new bonds in the investigated films which rendered the amorphous structure of the film as evident in the XRD pattern.

Other parameters that are associated with E_d, and E_o, are the interband transition strength moments, and are given by (Borah and Mostako 2020):

$$M_{-1} = \frac{E_d}{E_0}, M_{-3} = \frac{E_d}{E_0^3} \tag{10}$$

The calculated M_{-1} and M_{-3} values are displayed in Table 1. It is noted that S3 film exhibits the highest M_{-1} and M_{-3} values which confirm the increase in the electronic transitions probability due to the created charge transfer complex within the polymeric composite (Borah and Mostako 2020). Another parameter n_o, which is the extrapolated refractive index to infinite wavelength, is related to the dispersion and oscillator energies values via (Solomon et al. xxxx):

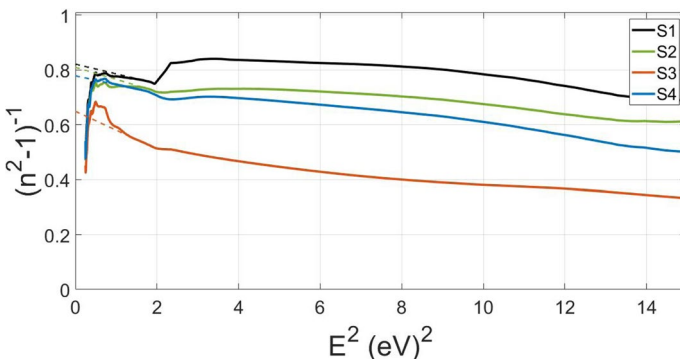$$n^2 = 1 + \frac{\left(n_o^2 - 1\right)E_M^2}{E_M^2 - E^2} \tag{11}$$

Fig. 13 Plot of the $\left(n^2 - 1\right)^{-1}$ *versus* E^2 relation (solid line), and the straight line fitting (dotted)

Table 1 Values of the optical parameters of the fabricated films

Sample	$S_o (nm^{-2})$	$\lambda_o (nm)$	$E_o = E_m (eV)$	$E_d (eV)$	$f (eV^2)$	M_{-1}	$M_{-3} (eV^{-2})$	n_o	$\frac{N}{m^*} \times 10^{57} (1/kg.m^3)$	ϵ_L	$w_p \times 10^{15} (Hz)$
S1	1.83×10^{-05}	257	4.81	5.85	28.18	1.217	0.0525	1.489	6	2.97	2.416
S2	1.47×10^{-05}	289	4.28	5.29	22.71	1.234	0.0671	1.494	5.11	3.10	2.184
S3	9.38×10^{-06}	405	3.06	4.71	14.42	1.539	0.1643	1.593	4.22	4.15	1.715
S4	2.067×10^{-05}	249	4.97	6.38	31.78	1.284	0.0518	1.511	1.46	2.77	1.236

where $E_M = E_o$ and $n_o = \sqrt{\frac{E_d}{E_o} + 1}$. The computed n_o values for the investigated films are displayed in Table 1, and it is found to increase with the addition of glycerin more than when adding acetic acid, which indicates that these optical parameters are closely related to the new structural modifications due to recent intermolecular bonds formed by the loaded additives inside the polymeric blend. On the other hand, the contributions of free carriers and the lattice vibration modes of dispersion are interrelated to the refractive index through the model in (Moustafa et al. 2019), where:

$$n^2 = \varepsilon_L - \frac{e^2 N}{4\pi^2 \varepsilon_o m^* c^2} \lambda^2 \tag{12}$$

where $e = 1.6 \times 10^{-19} C$ is the electron charge, and $\epsilon_o = 8.85 \times 10^{-12} F/m$ is the permittivity of free space. ϵ_L is the lattice dielectric constant, while N/m^* is the ratio of the free carrier concentration to the free carrier effective mass. The values of ϵ_L and N/m^* can be found by plotting the relation $n^2 - \lambda^2$ shown in Fig. 14, where a straight line fit is utilized to get ϵ_L and $\frac{N}{m^*}$ values. ϵ_L, and N/m^* values of the investigated films are listed in Table 1. It is evident from the obtained results that $n_o < \epsilon_L$, and this may be attributed to the free charge carrier contribution in the polarization process that occurs inside the polymeric composite films (Abdel-Khalek et al. 2021).

The obtained values of ϵ_L, and N/m^* are significant parameters for investigating the plasma resonance frequency of the polymeric film, w_p, that can be determined by (Mahmoud et al. 2021):

$$w_p = \sqrt{\frac{e^2}{\varepsilon_0 \varepsilon_L} \frac{N}{m^*}} \tag{13}$$

The obtained w_p values of the fabricated films are summarized in Table 1. The plasma resonance frequency is found to increase with the increase in the carrier concentration N/m^*. Notably, S3, and S4 films exhibits the lowest w_p values compared to plain PVA (S1). These results are mainly attributed to the contribution of the lattice vibration modes of the dispersion (Abdel-Khalek et al. 2021) due to the dopant of glycerol into the polymeric blend matrix. Additionally, according to the single-term Sellmeier
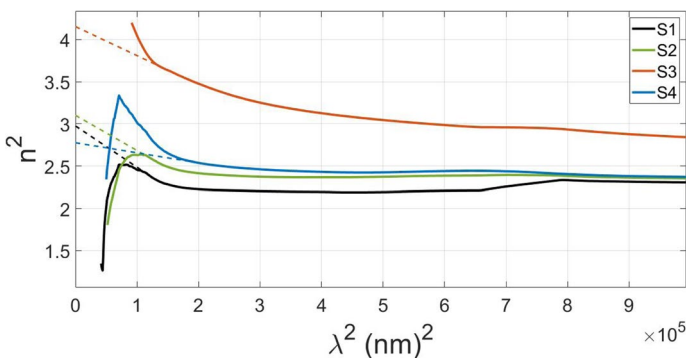

Fig. 14 Plot of the $n^2 versus \lambda^2$ relation (solid line), and the straightline fitting (dotted)

relation in the long wavelength range, the dispersion characteristics of the refractive index can be deduced through the following relation (Girgis et al. 2007):

$$n^2 - 1 = \frac{S_o \lambda_o^2}{1 - \frac{\lambda_o^2}{\lambda^2}} \tag{14}$$

where S_o is the average oscillator strength, and λ_o is the average interband oscillator wavelength. To get S_o and λ_o values, Eq. 14 is reformulated as:

$$\left(n^2 - 1\right)^{-1} = \frac{1}{S_o \lambda_o^2} - \frac{1}{S_o} \lambda^{-2} \tag{15}$$

After that, $(n^2 - 1)$ versus λ^{-2} diagram is plotted, then a straight line is fitted to the points in the long wavelength range, i.e., toward $\lambda^{-2} = 0$. The y-intercept and the slope of the straight line are used to attain the S_o and λ_o values. See Fig. 15. S_o and λ_o values of the investigated films are listed in Table 1. As observed, S_o and λ_o changed irregularly and were affected by the kind of additives to the PVA-PVP host. These changes may result from the charge transport complexes creation in the form of localized states in the PVA-PVP host matrix (Aziz et al. 2017). Furthermore, a similar behavior between S_o and E_d, can be observed for the investigated polymeric composites which indicates that strong interband optical transitions decrease the average oscillator strength (Borah and Mostako 2020).

5　Electronic losses and nonlinear optical studies

Electronic losses can be realized from the electron excitation spectra of the fabricated films, which are inferred from the complex permittivity function through different parameters. The first parameter related to losses is the loss tangent factor, tan (δ), that is defined as (Abdel Wahab et al. 2020):

$$\tan \delta = \frac{\varepsilon_i}{\varepsilon_r} \tag{16}$$
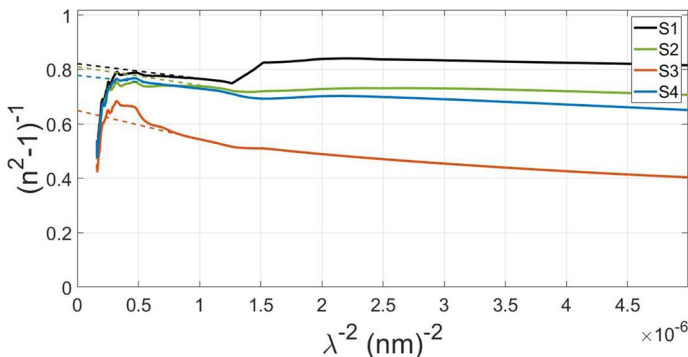
Fig. 15 The plot of $\left(n^2 - 1\right)^{-1}$ *versus* λ^{-2} relation (solid line), and the straightline fitting (dotted)

The loss tangent is an essential parameter that can be studied to denote the electronic losses of the fabricated films. The loss tangent factor is associated with the photons and electrons interactions inside the film and indicates the loss-rate of power due to oscillations of dipoles in a dissipative medium. Plot of the loss tangent as a function of the incident photon energy is given in Fig. 16. It is clearly shown that at photo energies greater than 1 eV, the fabricated films exhibit relatively very low dielectric loss values. This indicates that these polymeric composites possess good optical qualities due to the lower energy losses and lower scattering of the incident radiation. In the range E > 3eV, the loss tangent of S3 film starts to increase as the photon energy increases, while at E > 4eV, the loss tangent of S1, S2, and S4 films start to increase with the rise in photon energy. This response indicates the increment in the photons and electrons interactions originated in this wavelength range (Henry et al. 2021).

Other important parameters to evaluate the energy loss of electrons are the surface energy-loss function (SELF) and the volume energy-loss function (VELF). These energy loss functions are related to the complex permittivity values of the films through the following relations (Bhunia et al. 2021):

$$\text{SELF} = -\text{Im}\left(\frac{1}{\varepsilon}\right) = \frac{\varepsilon_i}{\left(\varepsilon_i^2 + \varepsilon_r^2\right)} \tag{17}$$

$$\text{VELF} = -\text{Im}\left(\frac{1}{\varepsilon + 1}\right) = \frac{\varepsilon_i}{\left(\varepsilon_i^2 + \left(\varepsilon_r + 1\right)^2\right)} \tag{18}$$

SELF and the VELF are two parameters indicating how the incident electromagnetic radiation interacts with electrons in the film when it transports through its surface or penetrates its mass (Bhunia et al. 2021). The dependence of SELF and VELF, on $h\nu$ is illustrated in Fig. 17a and b, respectively. It is clear that in the lower photon energy range, both functions decrease with increasing photon energy. Furthermore, $S2$ film exhibits the smallest losses expressed by the SELF and VELF in the telecommunications range around $E = 0.8eV$ or $\lambda = 1550nm$. The reduction in the SELF and VELF for S2 compared to S1 is approximately 60%. In the higher photon energy region, $1.8eV < E < 3.1eV$, an observation is the higher value of SELF as compared to VELF which indicates that the major loss energy from the surface is higher
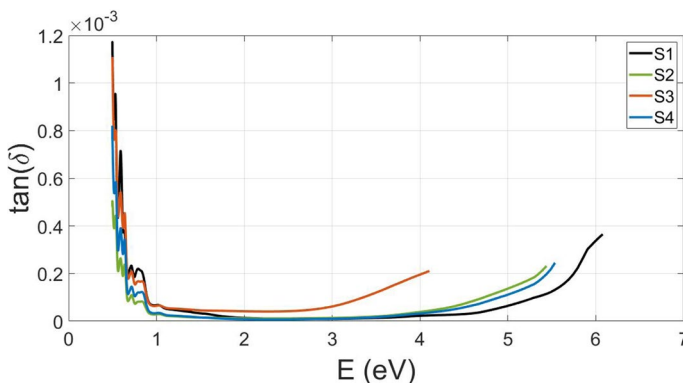

Fig. 16 The variation of the loss tangent with the photon energy (E) for the four fabricated samples

than those through the bulk. Generally, the loss due to the surface (SELF) is about 30% greater than that due to the bulk (VELF) for all the fabricated films. Furthermore, S1, S2 and S4 films show almost similar variation, for the SELF and the VELF values, versus the photon energy. However, S3 film shows much larger SELF and VELF values.

A final set of results to study is the nonlinear optical properties of the fabricated films. The nonlinear optical properties are essential parameters to offer an indication of the transfer efficiency and mobility of electron charge within the polymeric composites. That in turns; provides a sign to the potential use of the investigated composites in laser controlled applications (Elhosiny Ali et al. 2021), and optical switching devices (Hassanien et al. 2020). In this work, the study of the non-linear properties is done through three parameters that are interrelated to the dispersion parameters of the fabricated films: the first order susceptibility, $\chi^{(1)}$, the third-order susceptibility, $\chi^{(3)}$, and the nonlinear refractive index n_2. The first-order linear suscepti-bility can be calculated from E_d, and E_o (Priyadarshini et al. 2022):

(a)

(b)
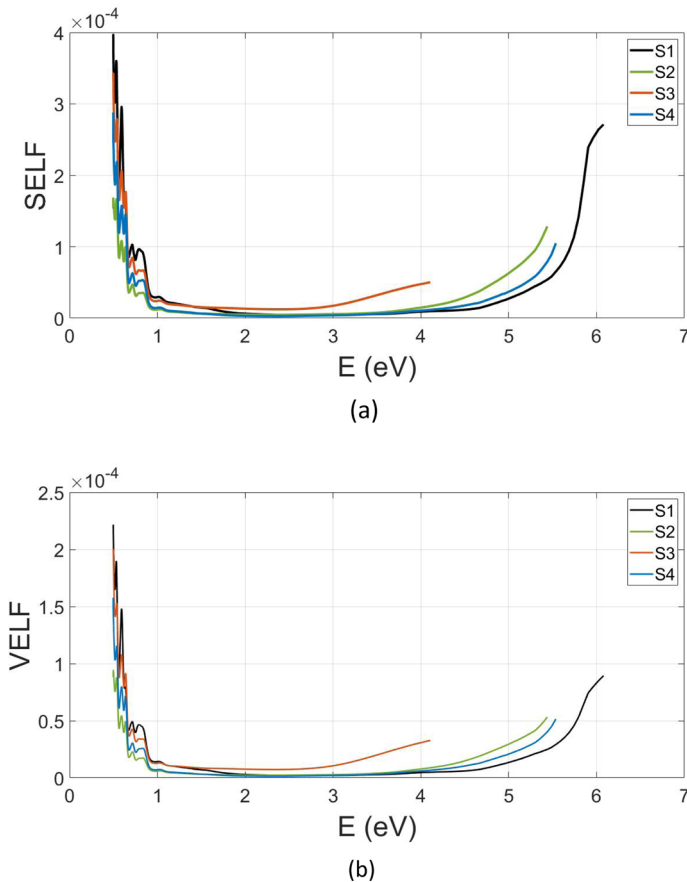
Fig. 17 Variation of (**a**) the surface energy-loss function and (**b**) the volume energy-loss function with the photon energy

$$\chi^{(1)} = \frac{1}{4\pi} \left[\frac{E_d}{E_0} \right] \tag{19}$$

Also, the third-order nonlinear susceptibility can be derived from the following relation (Priyadarshini et al. 2022):

$$\chi^{(3)} = \frac{A}{(4\pi)^4} \left[\frac{E_d}{E_0} \right]^4 \tag{20}$$

where $A = 1.7 x 10^{-10}$ e.s.u. (Priyadarshini et al. 2022). Finally, the nonlinear refractive index, n_2, can be obtained from the $\chi^{(3)}$, and n_o by the following expression (Priyadarshini et al. 2022):

$$n_2 = \frac{12\pi}{n_o} \chi^{(3)} \tag{21}$$

The values of $\chi^{(1)}$ for S1, S2, S3 and S4 films are 0.096, 0.098, 0.122, and 0.102, respectively, while the $\chi^{(3)}$ values are 1.50×10^{-14}, 1.588×10^{-14}, 3.839×10^{-14}, and 1.858×10^{-14} respectively. Also, n_2 values for S1, S2, S3 and S4 films are 3.799×10^{-13}, 4.008×10^{-13}, 9.086×10^{-13}, and 4.637×10^{-13} respectively. It can be noted that the values of the $\chi^{(1)}$ of the polymeric composites are higher than the plain PVA values. This reveals that the incorporation of the various additives to the polymeric host matrix increases the ability of the more electrons to transfer to upper levels by absorption of photon energies (Abdel-Aziz et al. 2021). Furthermore, the observed increase in the values of $\chi^{(3)}$ for $S2, S3,$ and $S4$ films over plain PVA $S1$ can be ascribed to increasing the electrons mobility and reducing the incident light deflection within the polymeric composites (Ali et al. 2021). Moreover, the comparison between $\chi^{(3)}$ values reveals that $S3$ film has the highest third-order susceptibility. Additionally, in comparison to several composite films in the literature, it is found that the nonlinear optical parameters of S3 film are relatively higher than those of the other polymeric-based, and metal-based composite films, as listed in Table 2. This suggests that the fabricated films could be promising materials for nonlinear optical applications.

6 Conclusion

In this work, new polymeric based films are introduced to serve as candidate platforms in the realm of optical applications. The proposed films include acetic acid and glycerin as embedded additives to a PVA/PVP polymeric blend host matrix. The films are investigated for optical reflectance and transmittance in the UV–vis-NIR range. Using the thin film model, the complex refractive index and the complex permittivity are calculated, and hence many other optical constants such as the dispersion parameters, interband transition strength moments, the loss tangent, the plasma resonance frequency, surface and volume energy loss functions and nonlinear optical properties.

The proposed films show many desirable improvements over plain PVA, and widely used materials in optical applications such as silicon dioxide. These advantages are higher refractive index which enables smaller device dimensions in integrated optics and small dispersion which is vital for long distance optical telecommunications. Furthermore, the fabricated films exhibit small optical losses along the investigated photon energy range,

Table 2 Reported values of the first order susceptibility, the third-order susceptibility, and the nonlinear refractive index, of various composite films with different filler materials

Composite Film	$\chi^{(1)}(esu)$	$\chi^{(3)}(esu)$	$n_2(esu)$	Reference
PVA/PVP	–	1.97×10^{-19}	7.17×10^{-18}	(Heiba et al. 2021a)
PVA/PVP/ZnO	–	2.20×10^{-19}	8.01×10^{-18}	(Heiba et al. 2021a)
PVA/PVP/ZnO/Co	–	18.25×10^{-19}	64.74×10^{-18}	(Heiba et al. 2021a)
PVA/PVP/ZnO/Cu	–	19.49×10^{-19}	69.09×10^{-18}	(Heiba et al. 2021a)
PVA/PVP/ZnO/Mn	–	35.82×10^{-19}	125.8×10^{-18}	(Heiba et al. 2021a)
PVA/PVP/ $Zn_{0.75}Cd_{0.25}S$	0.0203	11.47×10^{-22}	3.86×10^{-20}	(Heiba et al. 2022)
3.7 wt% Cu/PVA	0.089	10.7×10^{-15}	2.79×10^{-15}	(Ali et al. 2021)
PVA/PVP/SnS$_2$/Fe	0.040	4.1×10^{-16}	1.25×10^{-14}	(El-naggar et al. 2022d)
ZnO thin films	0.108	2.309×10^{-14}	5.668×10^{-13}	(Alsaad et al. 2020)
In-doped ZnO thin films	0.159	1.074×10^{-14}	2.339×10^{-13}	(Alsaad et al. 2020)
Ga-doped ZnO thin films	0.106	2.181×10^{-14}	5.375×10^{-13}	(Alsaad et al. 2020)

and an obvious enhancement in the nonlinear optical properties, suggesting the possibility of using these films in versatile nonlinear photonic applications.

Declarations

References

Abdel Wahab, E.A., Shaaban, K.S., Yousef, E.S.: Enhancement of optical and mechanical properties of sodium silicate glasses using zirconia. Opt. Quantum Electron. **52**, 1–19 (2020). https://doi.org/10.1007/s11082-020-02575-3

Abdel-Aziz, M.M., Algarni, H., Elhosiny Ali, H., Yahia, I.S., Khairy, Y., Zahran, H.Y., Abdel-lahi, M.O., Al-Hagan, O., Solyman, S.: A novel polymer/ceramic composite film for

different optical applications: optical linear, nonlinear, and limiting properties. Phys. Scr. **96**, 055804 (2021). https://doi.org/10.1088/1402-4896/abe88a

Abdel-Khalek, H., Amin, Fatma M., Wassel, Ahmed R., El-Mahalawy, Ahmed M.: Enhancement of structure and optical dispersion properties of N,N′-Bis(3-methylphenyl)-N,N′-diphenylbenzidine thin films: impact of UV irradiation. Opt. Mater. **113**, 110867 (2021). https://doi.org/10.1016/j.optmat.2021.110867

Abd-Elnaiem, A.M., Moustafa, S., Abdelraheem, A.M., Abdel-Rahim, M.A., Mahmoud, A.Z.: Effects of annealing on structural and optical properties of Ge20Se70Sn10 thin films for optoelectronic applications. J. Non. Cryst. Solids. **549**, 120353 (2020). https://doi.org/10.1016/j.jnoncrysol.2020.120353

Abdelrazek, E.M., Elashmawi, I.S., El-khodary, A., Yassin, A.: Structural, optical, thermal and electrical studies on PVA/PVP blends filled with lithium bromide. Curr. Appl. Phys. **10**, 607–613 (2010). https://doi.org/10.1016/j.cap.2009.08.005

Abdolrahimi, M., Seifi, M., Ramezanzadeh, M.H.: Study the effect of acetic acid on structural, optical and mechanical properties of PVA/chitosan/MWCNT films. Chinese J. Phys. **56**, 221–230 (2018). https://doi.org/10.1016/j.cjph.2017.12.018

Abdullah, O.G., Aziz, S.B., Omer, K.M., Salih, Y.M.: Reducing the optical band gap of polyvinyl alcohol (PVA) based nanocomposite. J. Mater. Sci. Mater. Electron. **26**, 5303–5309 (2015). https://doi.org/10.1007/s10854-015-3067-3

Akouibaa, A., Masrour, R., Benhamou, M., Derouiche, A., Ouarch, M.: Optical properties of Al_2O_3 thin films doped with hollow monometallic and core/shell bimetallic gold, silver nanoparticles. Opt. Quantum Electron. **54**, 1–17 (2022). https://doi.org/10.1007/S11082-022-04005-Y/FIGURES/9

Ali, F.M.: Structural and optical characterization of [(PVA:PVP)-Cu2+] composite films for promising semiconducting polymer devices. J. Mol. Struct. **1189**, 352–359 (2019). https://doi.org/10.1016/J.MOLSTRUC.2019.04.014

Ali, F.M., Kershi, R.M.: Synthesis and characterization of La3+ ions incorporated (PVA/PVP) polymer composite films for optoelectronics devices. J. Mater. Sci. Mater. Electron. **31**, 2557–2566 (2020). https://doi.org/10.1007/s10854-019-02793-w

Ali, H.E., Abdel-Aziz, M., Ibrahiem, A.M., Sayed, M.A., Hisham, S.M., Abd-Rabboh, N.S., Awwad, H., Algarni, M., Shkir, M., Khairy, M.Y.: Microstructure study and linear/nonlinear optical performance of bi-embedded PVP/PVA Films for optoelectronic and optical cut-off applications. Polymers **14**(9), 1741 (2022). https://doi.org/10.3390/polym14091741

Al-ramadhan, Z.A., Salman, J.A., Abdul, H., Hmud, K.: Optical and Morphological Properties of (PVA-PVP-Ag) Nanocomposites. Int. J. Sci. Res. **5**, 1828–1836 (2016). https://doi.org/10.21275/v5i3.nov161759

Alsaad, A.M., Ahmad, A.A., Qattan, I.A., Al-Bataineh, Q.M., Albataineh, Z.: Structural, optoelectrical, linear, and nonlinear optical characterizations of dip-synthesized undoped zno and group iii elements (B, al, ga, and in)-doped zno thin films. Crystals **10**(4), 252 (2020). https://doi.org/10.3390/cryst10040252

Aspnes, D.E., Studna, A.A.: Dielectric functions and optical parameters of Si, Ge, GaP, GaAs, GaSb, InP, InAs, and InSb from 1.5 to 6.0 eV. Phys. Rev. B **27**(2), 985–1009 (1983). https://doi.org/10.1103/PhysRevB.27.985

Aziz, S.B., Rasheed, M.A., Hussein, A.M., Ahmed, H.M.: Fabrication of polymer blend composites based on [PVA-PVP](1–x):(Ag2S)x (001 ≤ x ≤ 003) with small optical band gaps: Structural and optical properties. Mater. Sci. Semicond. Process. **71**, 197–203 (2017). https://doi.org/10.1016/j.mssp.2017.05.035

Aziz, S.B., Dannoun, E.M.A., Tahir, D.A., Hussen, S.A., Abdulwahid, R.T., Nofal, M.M., Abdullah, R.M., Hussein, A.M., Brevik, I: Synthesis of pva/CeO_2 based nanocomposites with tuned refractive index and reduced absorption edge: Structural and optical studies. Materials **14**(6), 1570 (2021). https://doi.org/10.3390/ma14061570

Badawi, A.: Engineering the optical properties of PVA/PVP polymeric blend in situ using tin sulfide for optoelectronics. Appl. Phys. A Mater. Sci. Process. **126**, 5 (2020). https://doi.org/10.1007/s00339-020-03514-5

Badawi, A.: Engineering the optical properties of PVA/PVP polymeric blend in situ using tin sulfide for optoelectronics. Appl. Phys. A Mater. Sci. Process. **126**, 1–12 (2020b). https://doi.org/10.1007/s00339-020-03514-5

Belhamra, S., Masrour, R., Hlil, E.K.: Dynamic phase transitions, electronic, and magnetic properties of Ba_2NiWO_6 and Sr_2NiWO_6 double perovskites. J. Supercond. Nov. Magn. **35**, 3613–3622 (2022). https://doi.org/10.1007/s10948-022-06405-3

Bhunia, A.K., Pradhan, S.S., Bhunia, K., Pradhan, A.K., Saha, S.: Study of the optical properties and frequency-dependent electrical modulus spectrum to the analysis of electric relaxation and conductivity effect in zinc oxide nanoparticles. J. Mater. Sci. Mater. Electron. 32, 22561–22578 (2021). https://doi.org/10.1007/s10854-021-06742-4

Boonsuk, P., Sukolrat, A., Kaewtatip, K., Chantarak, S., Kelarakis, A., Chaibundit, C.: Modified cassava starch/poly(vinyl alcohol) blend films plasticized by glycerol: structure and properties. J. Appl. Polym. Sci. 137, 48848 (2020). https://doi.org/10.1002/APP.48848

Borah, D.J., Mostako, A.T.T.: Investigation on dispersion parameters of molybdenum oxide thin films via wemple–didomenico (WDD) single oscillator model. Appl. Phys. A Mater. Sci. Process. 126, 1–13 (2020). https://doi.org/10.1007/s00339-020-03996-3

Cazón, P., Velazquez, G., Vázquez, M.: Novel composite films from regenerated cellulose-glycerol-polyvinyl alcohol: mechanical and barrier properties. Food Hydrocoll. 89, 481–491 (2019). https://doi.org/10.1016/J.FOODHYD.2018.11.012

Chaabouni, R., Ellouze, M., Hlil, E.K., Masrour, R., Jotania, R.: Role of nickel substitution in the structural, magnetic properties, and magnetocaloric effect in La0.67Ba0.22Sr0.11Mn0.95Ni00.5O₃ sample. J. Mater. Sci. Mater. Electron. 33, 23524–23541 (2022). https://doi.org/10.1007/S10854-022-09113-9/FIGURES/15

Chapalo, I., Theodosiou, A., Kalli, K., Kotov, O.: Multimode fiber interferometer based on graded-index polymer CYTOP fiber. J. Light. Technol. 38, 1439–1445 (2020). https://doi.org/10.1109/JLT.2019.2954286

Cholant, C.M., Rodrigues, M.P., Peres, L.L., Balboni, R.D.C., Krüger, L.U., Placido, D.N., Flores, W.H., Gündel, A., Pawlicka, A., Avellaneda, C.O.: Study of the conductivity of solid polymeric electrolyte based on PVA/GA blend with addition of acetic acid. J. Solid State Electrochem. 24, 1867–1875 (2020). https://doi.org/10.1007/s10008-020-04605-2

Choudhary, S.: Characterization of amorphous silica nanofiller effect on the structural, morphological, optical, thermal, dielectric and electrical properties of PVA–PVP blend based polymer nanocomposites for their flexible nanodielectric applications. J. Mater. Sci. Mater. Electron. 29, 10517–10534 (2018a). https://doi.org/10.1007/s10854-018-9116-y

Choudhary, S.: Structural, morphological, thermal, dielectric, and electrical properties of alumina nanoparticles filled PVA–PVP blend matrix-based polymer nanocomposites. Polym. Compos. 39, E1788–E1799 (2018b). https://doi.org/10.1002/pc.24793

Deshmukh, K., Ahamed, M.B., Sadasivuni, K.K., Ponnamma, D., AlMaadeed, M.A.A., Khadheer Pasha, S.K., Deshmukh, R.R., Chidambaram, K.: Graphene oxide reinforced poly (4-styrenesulfonic acid)/polyvinyl alcohol blend composites with enhanced dielectric properties for portable and flexible electronics. Mater. Chem. Phys. 186, 188–201 (2017). https://doi.org/10.1016/j.matchemphys.2016.10.044

Dhahri, I., Mabrouki, A., Ellouze, M., Dhahri, E., Labidi, S., Hlil, E.K., Masrour, R.: Simulation study by phenomenological and Bean-Rodbell methods of La0.7Sr0.3Mn0.95Fe00.5O₃ compound. Indian J. Phys. 96, 3509–3515 (2022). https://doi.org/10.1007/S12648-021-02275-Y/FIGURES/10

Dhayal, V., Hashmi, S.Z., Kumar, U., Choudhary, B.L., Dalela, S., Dolia, S.N., Alvi, P.A.: Optical and electrical properties of biocompatible and novel (CS–GO) polymer nanocomposites. Opt. Quantum Electron. 53, 1–13 (2021). https://doi.org/10.1007/s11082-020-02723-9

El Krimi, Y., Masrour, R.: Cobalt-based full Heusler compounds Co2FeZ (Z = Al, Si, and Ga): A comprehensive study of competition between XA and L21 atomic ordering with ab initio calculation. Mater. Sci. Eng. B. 284, 115906 (2022). https://doi.org/10.1016/J.MSEB.2022.115906

Elhosiny Ali, H., Algarni, H., Yahia, I.S., Khairy, Y.: Optical absorption and linear/nonlinear parameters of polyvinyl alcohol films doped by fullerene. Chinese J. Phys. 72, 270–285 (2021). https://doi.org/10.1016/j.cjph.2021.04.022

Elhosiny Ali, H., Abdel-Aziz, M.M., Yasmin Khairy, H.Y., Zahran, H. A., Yahia, I.S., El-Shamy, E.F., Sayed, M.A., Maged, F.A., Sanaa, M.F.: Microstructure analysis and nonlinear/linear optical parameters of polymeric composite films based PVAL for wide optical applications. Phys. Scripta 96(11), 115804 (2021). https://doi.org/10.1088/1402-4896/ac13e3

El-Kashef, H.: The necessary requirements imposed on polar dielectric laser dye solvents - II. Phys. B Condens. Matter. 311, 376–379 (2002). https://doi.org/10.1016/S0921-4526(01)00642-1

Elkoua, I.A., Masrour, R.: Structural, thermodynamics, optical, electronic, magnetic and thermoelectric properties of Heusler Ni₂MnGa: an ab initio calculations. Opt. Quantum Electron. 54, 1–18 (2022). https://doi.org/10.1007/S11082-022-03999-9/FIGURES/13

El-naggar, A.M., Heiba, Z.K., Kamal, A.M., Altowairqi, Y., Abd-Elkader, O.H., Mohamed, M.B.: Study the effect of loading non-stoichiometric zinc sulfide on optical characteristics of PVA/CMC/PVP blended polymer films. J. Polym. Res. 29, 1–15 (2022a). https://doi.org/10.1007/s10965-022-03256-3

El-naggar, A.M., Heiba, Z.K., Kamal, A.M., Altowairqi, Y., Mohamed, M.B.: Impact of loading PVA/CMC/PVP blend with CdS0.9M0.1 non-stoichiometrically doped by transition metals (M). Opt. Mater. **133**, 113085 (2022). https://doi.org/10.1016/j.optmat.2022.113085

El-naggar, A.M., Heiba, Z.K., Mohamed, M.B., Kamal, A.M., Abd-Elkader, O.H., Lakshminarayana, G.: Effect of ZnO/(Co or Mn) ratios on the structure and optical spectroscopy parameters of PVA/PVP/PEG blended polymer. Opt. Mater. **128**, 112411 (2022). https://doi.org/10.1016/j.optmat.2022.112411

El-naggar, A.M., Heiba, Z.K., Mohamed, M.B., Kamal, A.M., Osman, M.M., Albassam, A.A., Lakshminarayana, G.: Improvement of the optical characteristics of PVA/PVP blend with different concentrations of SnS2/Fe. J. Vinyl Addit. Technol. **28**, 82–93 (2022d). https://doi.org/10.1002/vnl.21868

Gad, M., Yevick, D.: Tunable polymer/silicon over insulator ring resonators. Opt. Eng. **47**, 124601 (2007). https://doi.org/10.1117/1.3050355

Gad, M., Yevick, D., Jessop, P.E.: Tunable polymer/silicon over insulator ring resonators. Opt. Eng. **47**, 124601 (2008). https://doi.org/10.1117/1.3050355

Gad, M., Yevick, D., Jessop, P.E.: High-speed polymer/silicon on insulator ring resonator switch. Opt. Eng. **47**, 094601 (2008). https://doi.org/10.1117/1.2978947

Gad, M., Yevick, D., Jessop, P.: Compound ring resonator circuit for integrated optics applications. J. Opt. Soc. Am. a. **26**, 2023 (2009). https://doi.org/10.1364/josaa.26.002023

Gad, M., Yevick, D., Jessop, P.: A comparison of modeling methods for ring resonator circuits. J. Opt. Soc. Am. a. **27**, 703 (2010). https://doi.org/10.1364/JOSAA.27.000703

Gad, M., Ackert, J., Yevick, D., Chrostowski, L., Jessop, P.: Ring resonator wavelength division multiplexing interleaver. J. Light. Technol. **29**, 2102–2108 (2011a). https://doi.org/10.1109/JLT.2011.2157081

Gad, M., Yevick, D., Jessop, P.: High sensitivity ring resonator gyroscopes. Fiber Integr. Opt. **30**, 395–410 (2011b). https://doi.org/10.1080/01468030.2011.611581

Gad, M., Zaki, A., Sabry, Y.M.: (2017) Silicon photonic mid-infrared grating coupler based on silicon-on-insulator technology. National Radio Science Conference. pp 400–406. doi: https://doi.org/10.1109/NRSC.2017.7893509

Girgis, S.Y., Salem, A.M., Selim, M.S.: Structural characterization and refractive index dispersion analysis of HgSe thin films grown by reactive solutions. J. Phys. Condens. Matter. **19**, 116213 (2007). https://doi.org/10.1088/0953-8984/19/11/116213

Hashim, A.: Enhanced Structural, optical, and electronic properties of In2O3 and Cr2O3 nanoparticles doped polymer blend for flexible electronics and potential applications. J. Inorg. Organomet. Polym. Mater. **30**, 3894–3906 (2020). https://doi.org/10.1007/s10904-020-01528-3

Hassanien, A.M., Atta, A.A., El-Nahass, M.M., Ahmed, S.I., Shaltout, A.A., Al-Baradi, A.M., Alodhayb, A., Kamal, A.M.: Effect of annealing temperature on structural and optical properties of gallium oxide thin films deposited by RF-sputtering. Opt. Quantum Electron. **52**, 1–16 (2020). https://doi.org/10.1007/s11082-020-02306-8

Heiba, Z.K., El-naggar, A.M., Mohamed, M.B., Altowairqi, Y., Kamal, A.M.: Noval properties of PVA/PVP polymer blend doped by nano-ZnO/M (M = Co, Cu, Mn, V). Appl. Phys. A Mater. Sci. Process. **127**, 1–12 (2021a). https://doi.org/10.1007/s00339-021-05129-w

Heiba, Z.K., Mohamed, M.B., Ahmed, S.I., Alhazime, A.A.: Tailoring the optical properties of PVA/PVP blend by doping with Cu/MnS nanoparticles. J. Vinyl Addit. Technol. **27**, 410–418 (2021b). https://doi.org/10.1002/vnl.21815

Heiba, Z.K., El-naggar, A.M., Mohamed, M.B., Kamal, A.M., Osman, M.M., Albassam, A.A., Lakshminarayana, G.: Modifications of the structural and optical properties of PVA/PVP loaded with Zn0.75-xCd0.25VxS nano powders. Opt. Quantum Electron. **54**, 1–16 (2022). https://doi.org/10.1007/s11082-022-03827-0

Henry, J., Sivakumar, G., Vettumperumal, R., Subramanian, T.S.S., Mohanraj, K.: Optical and photovoltaic properties of vacuum-evaporated CZTSe, CAZTSe, and AZTSe thin films: a comparative study. J. Mater. Sci. Mater. Electron. **32**, 20259–20272 (2021). https://doi.org/10.1007/s10854-021-06529-7

https://jascoinc.com/: Spectroscopy and Chromatography Instrumentation - JASCO

Jacob, W., vom Keudell, A., Schwarz-Selinger, T.: Infrared analysis of thin films: amorphous, hydrogenated carbon on silicon. Brazilian J. Phys. **31**, 109–109 (2001). https://doi.org/10.1590/s0103-97332001000100019

Jiang, Y., Liu, Y.Y., Liu, X., Lin, H., Gao, K., Lai, W.Y., Huang, W.: Organic solid-state lasers: a materials view and future development. Chem. Soc. Rev. **49**, 5885–5944 (2020). https://doi.org/10.1039/d0cs00037j

Jilani, W., Jlali, A., Guermazi, H.: Impact of CuO nanofiller on structural, optical and dielectric properties of CuO/DGEBA hybrid nanocomposites for optoelectronic devices. Opt. Quantum Electron. **53**, 1–17 (2021). https://doi.org/10.1007/s11082-021-03200-7

Kim, S.W., Lee, S.Y.: Transparent supercapacitors: from optical theories to optoelectronics applications. Energy Environ. Mater. **3**, 265–285 (2020). https://doi.org/10.1002/eem2.12095

Kim, E., Song, Y.C., Yeu, D.M., Shin, S.Y.: Low optical loss perfluorinated methacrylates for a single-mode polymer waveguide. Chem. Mater. **17**, 962–966 (2005). https://doi.org/10.1021/CM049933A/ASSET/IMAGES/MEDIUM/CM049933AN00001.GIF

Kleine, T.S., Frish, J.I., Pavlopoulos, N.G., Showghi, S.A., Himmelhuber, R., Norwood, R.A., Pyun, J.: Refractive index contrast polymers: photoresponsive systems with spatial modulation of refractive index for photonics. ACS Macro Lett. **9**, 416–421 (2020). https://doi.org/10.1021/acsmacrolett.9b00919

König, T.A.F., Ledin, P.A., Kerszulis, J., Mahmoud, M.A., El-Sayed, M.A., Reynolds, J.R., Tsukruk, V.V.: Electrically tunable plasmonic behavior of nanocube-polymer nanomaterials induced by a redox-active electrochromic polymer. ACS Nano **8**, 6182–6192 (2014). https://doi.org/10.1021/nn501601e

Labib, M., Gad, M., Sabry, Y.M., Khalil, D.: Strip Waveguide Enabling Low Loss for Silicon on Silica Technology in the MIR. In: proceedings - 2018 13th international conference on computer engineering and systems, ICCES 2018 (2019b)

Labib, M., Gad, M., Sabry, Y.M., Khalil, D.: Optimization of silicon on silica waveguides for mid-infrared applications at 4.28 um. Presented at the (2019a)

Lee, J.H., Chen, C.H., Lee, P.H., Lin, H.Y., Leung, M.K., Chiu, T.L., Lin, C.F.: Blue organic light-emitting diodes: current status, challenges, and future outlook. J. Mater. Chem. C. **7**, 5874–5888 (2019). https://doi.org/10.1039/c9tc00204a

Liang, D., Wang, X.Y.: Zoom optical system using tunable polymer lens. Opt. Commun. **371**, 189–195 (2016). https://doi.org/10.1016/J.OPTCOM.2016.03.074

Mahmoud, A.Z., Abdel-Rahim, M.A., Mohamed, M.: Role of the annealing temperature for optimizing the optical and electronic parameters of Ge10Se75Ag15 films for optoelectronic applications. Opt. Quantum Electron. **53**, 1–20 (2021). https://doi.org/10.1007/s11082-021-02832-z

Mahrous, H., Fedawy, M., El Sabbagh, M., Fikry, W., Gad, M.: Design of a 90 GHz SOI fin electro-optic modulator for high-speed applications. Appl. Sci. (2019). https://doi.org/10.3390/app9224917

Mahrous, H., Gad, M., Sabbagh, MEl., Fedawy, M., Fikry, W.: A high-speed electro-optic modulator with optimized electrode positions. Proc Int Conf. Comput. Eng. Syst. ICCES **2018**, 530–535 (2019). https://doi.org/10.1109/ICCES.2018.8639436

Mahrous, H., Azmy, M., Afifi, A., Abouelainain, A., Kotb, A., Fedawy, M., Fikry, W., Gad, M., Selim, D.: Design of compact, high-speed and low-loss silicon-on-silica electro-optic modulators. Semicond. Sci. Technol. **35**, 095017 (2020). https://doi.org/10.1088/1361-6641/AB9D09

Mahrous, H., Fedawy, M., El Sabbagh, M., Fikry, W., Gad, M.: 130 Gbps low-loss electro-optic modulator based on metal-oxide-semiconductor technology. Optik (Stuttg). **217**, 164928 (2020). https://doi.org/10.1016/J.IJLEO.2020.164928

Mahrous, H., Fedawy, M., El Sabbagh, M., Fikry, W., Gad, M.: A compact 120 GHz monolithic silicon-on-silica electro-optic modulator. Opt. Quantum Electron. (2020c). https://doi.org/10.1007/s11082-020-2239-4

Mansur, H.S., Sadahira, C.M., Souza, A.N., Mansur, A.A.P.: FTIR spectroscopy characterization of poly (vinyl alcohol) hydrogel with different hydrolysis degree and chemically crosslinked with glutaraldehyde. Mater. Sci. Eng. C. **28**, 539–548 (2008). https://doi.org/10.1016/j.msec.2007.10.088

Masrour, R., Kadim, G., Jabar, A., Hlil, E.K., Ellouze, M.: Emerging opportunities for Sr_2FeReO_6 and Sr_2CrWO_6 double perovskites in potential magnetic refrigerants and spintronics in room temperature regime. Appl. Phys. A Mater. Sci. Process. **128**, 1–8 (2022). https://doi.org/10.1007/S00339-022-06152-1/FIGURES/11

Mohammed, M.I., Yahia, I.S., El-Mongy, S.A.: Studying the structural, optical, electrical properties and magnetic properties of Fe3+-codoped Al3+/PVA flexible composite films. Opt. Quantum Electron. **54**, 1–23 (2022). https://doi.org/10.1007/s11082-022-03981-5

Mohanapriya, M.K., Deshmukh, K., Chidambaram, K., Ahamed, M.B., Sadasivuni, K.K., Ponnamma, D., AlMaadeed, M.A.A., Deshmukh, R.R., Pasha, S.K.K.: Polyvinyl alcohol (PVA)/polystyrene sulfonic acid (PSSA)/carbon black nanocomposite for flexible energy storage device applications. J. Mater. Sci. Mater. Electron. **28**, 6099–6111 (2017). https://doi.org/10.1007/s10854-016-6287-2

Mohsin, M., Hossin, A., Haik, Y.: Thermal and mechanical properties of poly(vinyl alcohol) plasticized with glycerol. J. Appl. Polym. Sci. **122**, 3102–3109 (2011). https://doi.org/10.1002/app.34229

Morsi, M.A., Abdelrazek, E.M., Ramadan, R.M., Elashmawi, I.S., Rajeh, A.: Structural, optical, mechanical, and dielectric properties studies of carboxymethyl cellulose/polyacrylamide/lithium titanate nanocomposites films as an application in energy storage devices. Polym. Test. **114**, 107705 (2022). https://doi.org/10.1016/j.polymertesting.2022.107705

Moustafa, S., Mohamed, M., Abdel-Rahim, M.A.: Composition dependence of structural and optical properties of GexSe100−x semiconducting thin films. Opt. Quantum Electron. **51**, 1–19 (2019). https://doi.org/10.1007/s11082-019-2049-8

Naik, R., Aparimita, A., Alagarasan, D., Varadharajaperumal, S., Ganesan, R.: Linear and nonlinear optical properties change in Ag/GeS heterostructure thin films by thermal annealing and laser irradiation. Opt. Quantum Electron. **52**, 1–18 (2020). https://doi.org/10.1007/s11082-020-2245-6

Nocentini, S., Riboli, F., Burresi, M., Martella, D., Parmeggiani, C., Wiersma, D.S.: Three-dimensional photonic circuits in rigid and soft polymers tunable by light. ACS Photonics **5**, 3222–3230 (2018). https://doi.org/10.1021/acsphotonics.8b00461

Oh, M.C., Chu, W.S., Shin, J.S., Kim, J.W., Kim, K.J., Seo, J.K., Lee, H.K.H.J., Noh, Y.O., Lee, H.K.H.J.: Polymeric optical waveguide devices exploiting special properties of polymer materials. Opt. Commun. **362**, 3–12 (2016). https://doi.org/10.1016/j.optcom.2015.07.079

Othayoth, A.K., Srinivas, B., Murugan, K., Muralidharan, K.: Poly(methyl methacrylate)/polyphosphate blends with tunable refractive indices for optical applications. Opt. Mater. **104**, 109841 (2020). https://doi.org/10.1016/j.optmat.2020.109841

Pina-Hernandez, C., Koshelev, A., Digianantonio, L., Dhuey, S., Polyakov, A., Calafiore, G., Goltsov, A., Yankov, V., Babin, S., Cabrini, S., Peroz, C.: Printable planar lightwave circuits with a high refractive index. Nanotechnology. **25**, 325302 (2014). https://doi.org/10.1088/0957-4484/25/32/325302

Priyadarshini, P., Sahoo, D., Naik, R.: A review on the optical properties of some germanium based chalcogenide thin films and their applications. Opt. Quantum Electron. **54**, 1–26 (2022). https://doi.org/10.1007/s11082-022-03564-4

Raïâ, M.Y., Masrour, R., Hamedoun, M., Kharbach, J., Rezzouk, A., Hourmatallah, A., Benzakour, N., Bouslykhane, K.: Stability, magnetic, electronic, elastic, thermodynamic, optical, and thermoelectric properties of CO_2TiSn, CO_2ZrSn and CO_2HfSn Heusler alloys from calculations using generalized gradient approximation techniques. J. Mater. Sci. Mater. Electron. **33**(25), 20229–20256 (2022). https://doi.org/10.1007/s10854-022-08841-2

Raïâ, M.Y., Masrour, R., Hamedoun, M., Kharbach, J., Rezzouk, A., Hourmatallah, A., Benzakour, N., Bouslykhane, K.: Effect of L21 and XA ordering on structural, martensitic, electronic, magnetic, elastic, thermal and thermoelectric properties of CO_2FeGe Heusler alloys. Solid State Commun. **355**, 114932 (2022). https://doi.org/10.1016/J.SSC.2022.114932

Rheims, J., Köser, J., Wriedt, T.: Refractive-index measurements in the near-IR using an Abbe refractometer. Meas. Sci. Technol. **8**, 601–605 (1997). https://doi.org/10.1088/0957-0233/8/6/003

Sakli, A., Amri, R., Lelong, A., Gamra, D., Bouchriha, H., Lejeune, M., Clin, M.: Optical properties of polymerized ethylene thin films deposited by PECVD technique. Opt. Quant. Electron. **53**, 1–13 (2021). https://doi.org/10.1007/s11082-021-03194-2

Shalaby, R.A., Selim, M.A., Adib, G.A., Sabry, Y.M., Gad, M., Khalil, D.: Silicon photonics dual-coupler nested coupled cavities. Presented at the (2019)

Shalaby, R.A., Adib, G., Sabry, Y.M., Gad, M., Khalil, D., Sabry, Y.M., Khalil, D.: Silicon photonic coupled-ring resonator in nested configuration comprising different length scales. Presented at the (2020)

Shen, K., Baig, S., Jiang, G., Paik, Y. Hun., Kim, S.J., Wang, M.R.: Improved light emitting UV curable PbS quantum dots-polymer composite optical waveguides. Opt. Commun. **402**, 606–611 (2017). https://doi.org/10.1016/J.OPTCOM.2017.06.083

Siva, V., Vanitha, D., Murugan, A., Shameem, A., Bahadur, S.A.: Studies on structural and dielectric behaviour of PVA/PVP/SnO nanocomposites. Compos. Commun. **23**, 100597 (2021). https://doi.org/10.1016/j.coco.2020.100597

Solomon, I., Schmidt', M.P., Senemaud, C., Driss Khodja, M.: Band structure of carbonated amorphous silicon studied by optical, photoelectron, and x-ray spectroscopy.

Sreekanth, K., Siddaiah, T., Gopal, N.O., Madhava Kumar, Y., Ramu, C.: Optical and electrical conductivity studies of VO^{2+} doped polyvinyl pyrrolidone (PVP) polymer electrolytes. J. Sci. Adv. Mater. Devices. **4**, 230–236 (2019). https://doi.org/10.1016/j.jsamd.2019.06.002

Tan, D.Q.: Review of polymer-based nanodielectric exploration and film scale-up for advanced capacitors. Adv. Funct. Mater. **30**, 1808567 (2020). https://doi.org/10.1002/adfm.201808567

Tang, Y., Cabrini, S., Nie, J., Pina-Hernandez, C.: High-refractive index acrylate polymers for applications in nanoimprint lithography. Chin. Chem. Lett. **31**, 256–260 (2020). https://doi.org/10.1016/j.cclet.2019.04.012

Wei, G.Q., Wang, X.D., Liao, L.S.: Recent advances in 1D organic solid-state lasers. Adv. Funct. Mater. **29**, 1902981 (2019). https://doi.org/10.1002/adfm.201902981

Wemple, S.H., DiDomenico, M., Bel, J.: Behavior of the electronic dielectric constant in covalent and ionic materials. Phys. Rev. B **3**(4), 1338 (1971)

Wooten, F.: Optical properties of solids. (1972)

Yalagala, B., Khandelwal, S., Badhulika, S.J.D.: Wirelessly destructible MgO-PVP-Graphene composite based flexible transient memristor for security applications. Mater. Sci. Semicond. Process. **104**, 104673 (2019). https://doi.org/10.1016/j.mssp.2019.104673

Yang, D., Ma, D.: Development of organic semiconductor photodetectors: from mechanism to applications. Adv. Opt. Mater. **7**, 1–23 (2019). https://doi.org/10.1002/adom.201800522

Zappe, H.: Fundamentals of micro-optics Technology, devices and applications. (2010)